

Augmenting Reinforcement Learning with Transformer-based Scene Representation Learning for Decision-making of Autonomous Driving

Haochen Liu, Zhiyu Huang, Xiaoyu Mo, and Chen Lv*, *Senior Member, IEEE*

Abstract—Decision-making for urban autonomous driving is challenging due to the stochastic nature of interactive traffic participants and the complexity of road structures. Although reinforcement learning (RL)-based decision-making scheme is promising to handle urban driving scenarios, it suffers from low sample efficiency and poor adaptability. In this paper, we propose Scene-Rep Transformer to improve the RL decision-making capabilities with better scene representation encoding and sequential predictive latent distillation. Specifically, a multi-stage Transformer (MST) encoder is constructed to model not only the interaction awareness between the ego vehicle and its neighbors but also intention awareness between the agents and their candidate routes. A sequential latent Transformer (SLT) with self-supervised learning objectives is employed to distill the future predictive information into the latent scene representation, in order to reduce the exploration space and speed up training. The final decision-making module based on soft actor-critic (SAC) takes as input the refined latent scene representation from the Scene-Rep Transformer and outputs driving actions. The framework is validated in five challenging simulated urban scenarios with dense traffic, and its performance is manifested quantitatively by the substantial improvements in data efficiency and performance in terms of success rate, safety, and efficiency. The qualitative results reveal that our framework is able to extract the intentions of neighbor agents to help make decisions and deliver more diversified driving behaviors.

Index Terms—Autonomous driving, decision-making, reinforcement learning, scene representation.

I. INTRODUCTION

Making safe, smooth, and intelligent decisions is a major challenge for autonomous vehicles (AVs) [1], [2], especially under complex urban driving scenarios [3], primarily due to the nature of sophisticated interaction dynamics among various traffic participants and road structures. This gives rise to the reinforcement learning (RL)-based methods, which are becoming more and more popular in use [4]–[6]. Thanks to the learning ability of RL agents through interactions with the driving environments (mostly in simulation), researchers and engineers are liberated from burdensome rule-based decision schemes and the AV is more capable of handling diverse traffic situations and tasks [7], [8]. However, RL-based approaches still encounter some common issues that may strike its further development. One leading drawback is data efficiency, which means training a functional driving policy requires a massive amount of samples through interactions with the environment.

H. Liu, Z. Huang, X. Mo, and C. Lv are with the School of Mechanical and Aerospace Engineering, Nanyang Technological University, 639798, Singapore. (E-mails: haochen002@e.ntu.edu.sg, zhiyu001@e.ntu.edu.sg, xiaoyu006@e.ntu.edu.sg, lyuchen@ntu.edu.sg)

This work was supported by the SUG-NAP Grant (No. M4082268.050) of Nanyang Technological University, Singapore.

*Corresponding author: C. Lv

This problem becomes harsher when facing the urban driving scenarios, such as crossing the unprotected left turn or nudging in road branches with dense traffic. Another problem is how to construct and encode the state representation of urban driving scenarios, which is a bottleneck in generalizing RL to more complex scenes. Unlike common RL problems where the state of the environment or agent is relatively simple, state representations for urban driving should cover heterogeneous information such as dynamic features among traffic flows, latent agent interactions, and road structures. Moreover, we believe it is beneficial to distill the predictive information in the scene representation, which could help the agent understand the consequences under certain driving actions, thus facilitating the learning of driving policies for decision making.

Accordingly, this paper proposes a Transformer-based structure (named Scene-Rep Transformer) to better capture the relations of the heterogeneous elements and inject predictive information into the scene representation, in order to augment the ability of the RL-based decision-making scheme and speed up training. First off, we construct a multi-stage Transformer (MST), which encodes the raw heterogeneous scene elements' information (e.g., the agent's historical motion states and candidate route waypoints) and fuse the information to represent the interactions between them. The MST would yield a single latent feature vector about the driving scene at a given time step. Then, we introduce the sequential latent Transformer (SLT) to distill the common features from a sequence of latent-action pairs from future steps into the latent at the current step, using a self-supervised learning method. The purpose of SLT is to acquire a core understanding of the sequential dynamics of the environment and thus reduce the exploration space because the current latent representation contains the consistent information of future steps. The SLT is only used in the training process to facilitate the learning of latent vectors and speed up training. Eventually, the SAC-based decision-making module would take as input the refined latent feature vector and outputs better-quality decisions. The main contributions of this paper can be outlined as follows:

- 1) A novel Transformer-based scene representation learning framework is designed to effectively augment the ability of RL-based decision-making systems (both training and testing) in urban driving scenarios.
- 2) A multi-stage Transformer is proposed to encode the information of heterogeneous scene elements and model the interactions among agents and map waypoints, yielding a latent scene representation for the RL module. A sequential latent Transformer with an augmented self-supervised learning objective is proposed to distill the

predictive sequential information into the latent representation to facilitate RL training.

- 3) The proposed framework is validated under multiple demanding urban driving scenarios and shows a significant effect in improving the RL driving agent’s performance in terms of data efficiency, task success rates, and interpretability. The effects of different components of our framework are also investigated.

II. RELATED WORK

A. Reinforcement Learning for Autonomous Driving

Reinforcement learning (RL) recently has been widely employed in decision-making tasks for autonomous driving to good effect [4], outcompeting the rule-based approaches that are usually onerous and cannot function well in complex tasks [2]. Another competitive approach is imitation learning [9], [10], which relies on supervised learning with expert data, but it suffers from the distributional shift problem in the deployment. On the other hand, RL can avoid this problem because it relies on interacting with the environment but may require a massive amount of interactions to train an acceptable policy. Therefore, recent works have proposed some methods to improve the data efficiency of RL, such as guiding the RL decision-making with expert actions [5], [11], [12] as it can significantly reduce the action exploration space. In our work, rather than using expensive expert guidance or demonstration, we propose to leverage the representation learning technique to obtain a better, predictive, and generalizable representation of the environment, in order to improve the training data efficiency and testing performance of RL. Another problem with the current RL methods for autonomous driving is that they focus on low-level decisions and end-to-end controls [8], such as controlling the steering wheel [13], however, low-level decision-making is not generalizable and robust. Therefore, in our work, we apply the RL method for high-level decision-making tasks [14] in various autonomous driving scenarios, which shows promising results.

B. Representation Learning in Reinforcement Learning

A good scene representation is crucial to help the agent better understand the complex environment and improve decision-making abilities. The driving scene with multi-modal information (e.g., map and traffic agents) inputs is initially be represented in a rasterization format (images), which has been used in visual-based driving systems and shows simplicity and adaptation. However, rasterized images inevitably lose the explicit relations between the agents and map [15], which may cost a large network and more data to recover certain relations. An alternative approach is the concise and unified vectorized representation for both traffic agents and road maps [16], which is widely applied in motion forecasting research [17]. In our work, we employ the vectorized representation that unifies the positions of agents and waypoints of maps under the same coordinate system. Another important point for scene representation is modeling the interactions between different elements (e.g., agent-agent and agent-map). Some works have explored graph neural networks (GNNs) in the RL framework

to formulate the interactions between multiple agents. For example, DeepScene-Q [18] introduced GNN-based encoder modeling interactions for urban driving decision-making. DQ-GAT further improved the DeepScene-Q method by introducing the graph attention network (GAT) [19]. In this work, we employ a more powerful Transformer-based structure for interaction modeling, which has been widely used for encoding the environment in the motion forecasting field [17], [20], [21]. We also propose to incorporate the candidate route waypoints to the scene representation, making the map information more correlated to the decision-making tasks.

In addition to more effective environment encoding, another aspect to elevate the performance of RL through representation learning is to distill the predictive knowledge of environmental dynamics into the latent representation. Global value function (GVF) provides a predictive value for scene representations [22], but may face importance sampling issues and have limited improvement facing with sparse reward in complex urban scenes. [23] proposed a model-based imitative method to learn the global predictive knowledge from latent space. Further, an augmentation method for learning self-consistency [24] latent representation is proposed in DrQ [25] and CURL [26] and has been applied in image-based driving systems. Self latent consistency is initially acquired through autoencoder-based approaches [27] by introducing the reconstruction loss, which imposes a great amount of computation burden on the system. In contrast, the self-supervised representation learning method, eliminates the reconstruction loss with directly self latent state pairing through a Siamese encoder [28]. However, most of the self-supervised approaches only consider the current or uni-step consistency to the prediction of global dynamics; yet the sequential consistency is another key factor for better representations under the partially observable environment. Therefore, in this work, we construct an augmentation method for representation learning and follow the idea of self-predictive representations (SPR) [29], which achieves excellent performance in Atari games. Rather than using a recurrent structure for global prediction, we adopt a Transformer-based structure to better adapt to the partially observable environment for urban autonomous driving.

III. REINFORCEMENT LEARNING WITH SCENE-REP TRANSFORMERS

A. Framework

The proposed RL framework focuses on making smart decisions given a complex state-input representing the dynamics and map information of the autonomous driving agent and its neighbors. This section provides an overview of the proposed framework, which consists of three main parts, as shown in Fig. 1. The multi-stage Transformer takes as input the vectorized scene representation, encoding the information and interactions among agents, and outputs a latent feature vector. The sequential latent Transformer then takes consecutive latent feature vectors across time together with corresponding action embeddings and outputs a sequence of predictive latent vectors, which are trained with the sequential consistency. The soft-actor-critic-based decision-making module finally takes

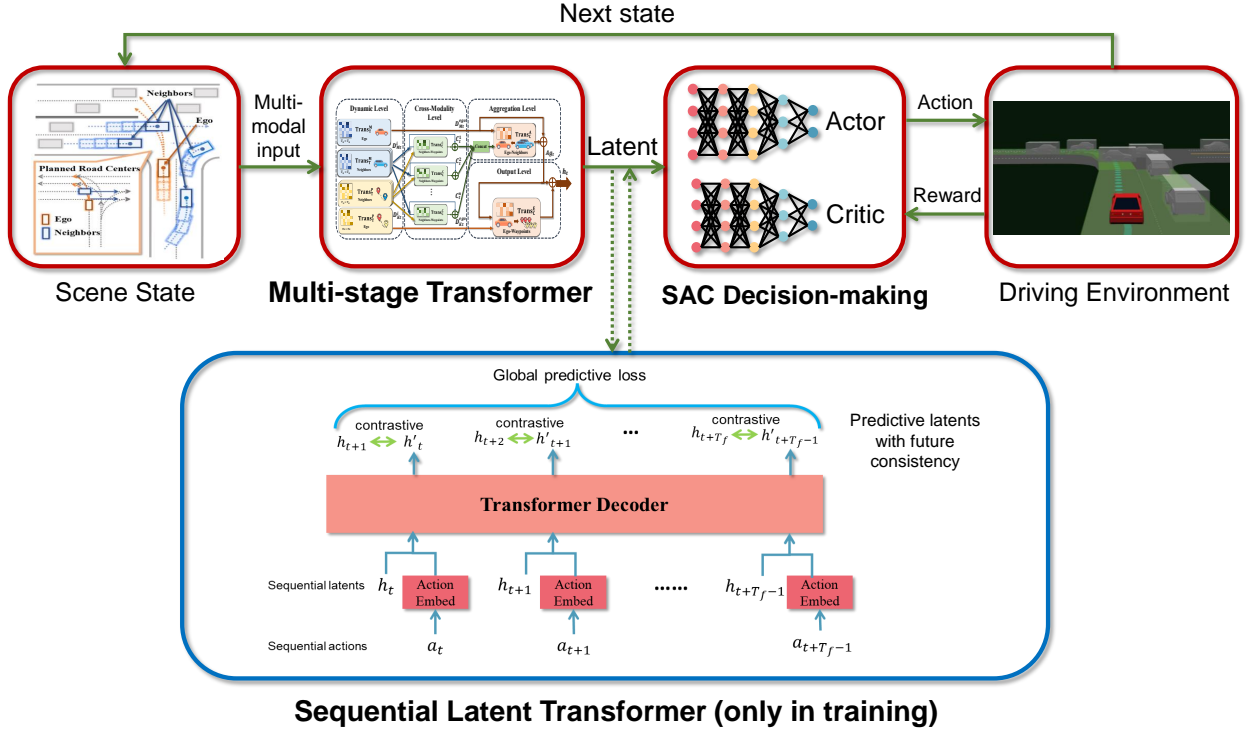


Fig. 1. An overview of our RL framework with Scene-Rep Transformer. Given vectorized scene inputs, the multi-stage Transformer encodes the multi-modal information with interaction awareness. A sequential latent Transformer performs the self-supervised representation learning by consecutive latent action pairs for predictive latents with future consistency. The soft-actor-critic module takes the latent feature vector for making driving decisions.

the latent vector from the scene encoder and outputs driving actions. The trained multi-stage transformer and decision module are used during the inference (deployment) phase, while the sequential latent Transformer is only employed in the training phase.

Problem Formulation: Two objectives are considered during the learning process. For RL decision-making, the objective follows the Markov decision process (MDP) represented as a tuple $(s_t, a_t, r_t, s_{t+1}, \gamma)$. Specifically, the self-driving agent receives state representation $s_t \in \mathcal{S}$ from the environment and executes an action $a_t \in \mathcal{A}$ according to its policy $\pi(a_t|s_t)$. The environment then returns a reward $r_t(s_t, a_t)$ and transitions to the next state $s_{t+1} \in \mathcal{S}$. The goal of RL is to optimize the policy π so as to maximize the expected cumulative discounted returns: $\max \mathbb{E}_\pi [\sum \gamma^t r_t]$. The objective of self-supervised learning in the sequential latent Transformer module is to enforce the sequential similarities between the predicted latent h'_t and the future ground-truth one h_{t+1} over a global predictive horizon T_G : $\min \frac{1}{T_G} \sum_t \mathcal{L}_{sim}(h'_t, h_{t+1})$.

State representations: At a time step t , the state input s_t encompasses the historical motion states of all agents and their local candidate route waypoints:

$$s_t = [\mathcal{M}_t; \mathcal{K}_t],$$

where $\mathcal{M}_t = \{M_t^{ego}, M_t^1, M_t^2, \dots, M_t^n\}$ contains historical motion trajectories of the controlled ego vehicle M_t^{ego} and nearby n vehicles $M_t^{1:n}$ within a certain distance d_n . Each motion trajectory is a sequence of motion states of certain vehicle over historical horizon T_h : $M_t =$

$\{m_{t-T_h+1}, m_{t-T_h+2}, \dots, m_t\}$, and each motion state m_t includes positions, velocities, and heading angles: $m_t = (x_t, y_t, v_{x_t}, v_{y_t}, \psi_t)$. \mathcal{K}_t represents candidate routes, $\mathcal{K}_t = \{K_t^{ego}, K_t^1, K_t^2, \dots, K_t^n\}$ corresponding to different agents in the scene. The candidate route waypoints K_t^{ego}, K_t^n for each agent consists of a set of local candidate route sequences ahead of its current position $K_t^n = \{\mathbf{k}_t^{n,1}, \mathbf{k}_t^{n,2}, \dots\}$. Each local candidate route is composed of a sequence of waypoints across the future horizon T_K : $\mathbf{k}_t = \{k_t, \dots, k_{t-T_K}\}$, where $k_t = (w_{x_t}, w_{y_t}, w_{\psi_t})$ is the position and heading angle of a waypoint. It is a succinct representation of an agent's intention since it can outline the agent's future positions through the attention mechanism and improve the interpretability of decision-making. The state representation s_t is encoded by the proposed multi-stage Transformer, followed by an off-policy RL algorithm for decision-making.

B. Multi-stage Transformer

The architecture of multi-stage Transformer (MST) functions as a hierarchical encoder to map the scene states s_t to a latent representation: $h_t \leftarrow \Phi_{MST}(s_t)$. The structure is designed following the intuitions that 1) the model should be interaction-aware to handle interactions among agents in the driving scene; 2) the model should consider different modalities of interactions. Therefore, a Transformer-based network is employed to model the interactions among the map and agents in the driving scene, and a multi-stage structure is implemented for explicitly encoding the different modalities of interactions. The proposed MST structure for state encoding benefits the

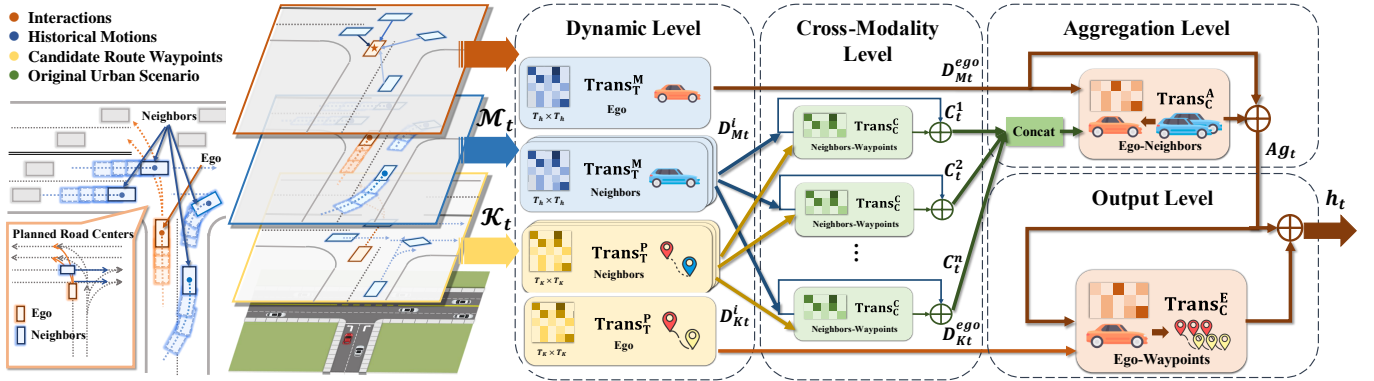


Fig. 2. An overview of the MST Structure. The urban scenario on the left side can be layered to explicit representations s_t as the historical motion states \mathcal{M}_t and candidate route waypoints \mathcal{K}_t . The implicit layer for agent interactions are modeled in the subsequent multi-stage structure: **1) Dynamic level** encodes \mathcal{M}_t and \mathcal{K}_t along temporal axis; **2) Cross-modality level** models the interactions of neighbor agents, which are aggregated to the ego agent through **3) Aggregation level**; **4) Output level** adds the ego-waypoints and ego-neighbor interaction features to output the latent representation h_t .

learning of latent representations in several ways: 1) the underlying dynamics of the driving scene is better captured; 2) the candidate route information is effectively leveraged for the guidance of future intentions; 3) the computation efficiency is guaranteed due to the quadratic complexity of the Transformer network; 4) the attention mechanism can perfectly deal with the varying number of agents in the scene, with excellency in interpretability.

We will first introduce the multi-head attention, which is the core mechanism in the proposed MST structure for representing the interactions inside the Transformer at different levels.

$$\text{MHA}(\mathbf{Q}, \mathbf{K}, \mathbf{V}, \mathbf{M}) = \text{concat}(\text{head}_1, \dots, \text{head}_h)W^O, \quad (1)$$

where the attention results from h heads are concatenated to capture different aspects of information. Each head captures the attention weighted value given $\mathbf{Q}, \mathbf{K}, \mathbf{V}$ denoting query, key, and value transformed by matrices W_i^Q, W_i^K, W_i^V :

$$\text{head}_i = \text{Att}(\mathbf{Q}W_i^Q, \mathbf{K}W_i^K, \mathbf{V}W_i^V, \mathbf{M}). \quad (2)$$

The attention weighted values are calculated by scaled dot-product with attention mask \mathbf{M} :

$$\text{Att}(\mathbf{Q}, \mathbf{K}, \mathbf{V}, \mathbf{M}) = \text{softmax}\left(\frac{\mathbf{Q}\mathbf{K}^T}{\sqrt{d_k}} \cdot \mathbf{M}\right) \mathbf{V}, \quad (3)$$

where d_k is the dimension of key. Attention mask $\mathbf{M} \in d_q \times d_k$ enables varying numbers of agents, and thus the highly dynamic nature of urban scene is well-adapted across different elements and time steps.

Next, we will provide the detailed MST multi-stage structure, as illustrated in Fig.2. The framework follows the subsequent computational flow: 1) dynamic level that encodes the representations of agents' historical motions and candidate route waypoints separately; 2) cross-modality level that models the cross-modal interactions among agents and their candidate route waypoints; 3) aggregating level that composites the second level latent of neighbor agents to the ego; 4) output level

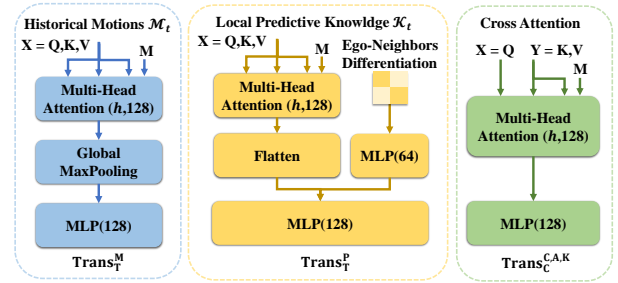


Fig. 3. The structures of networks along different axis in our proposed MST.

that queries the candidate route waypoints for the ego agent from the third stage, concatenating with selected information flow. Each level of encoding is detailed as below.

1) *Dynamic Level*: Given input state s_t , dynamic level separately encodes the historical motions \mathcal{M}_t and corresponding local candidate waypoints \mathcal{K}_t for each vehicle. Hereby we introduce a single layer Transformer along the temporal axis for dynamic level encoding.

$$\text{Trans}_T^M(\mathbf{X}, \mathbf{M}) = \text{MLP}(\text{MaxPool}(\text{MHA}(\mathbf{X}, \mathbf{M}))), \quad (4)$$

where the input $\mathbf{X} = \mathbf{Q}, \mathbf{K}, \mathbf{V}$ denoting the self-attention mechanism for temporal features, and max pooling is adopted to prevent over-fitting.

To distill the temporal feature for candidate route waypoints, the vehicle embedding \mathbf{Emb} is concatenated to differentiate the categorical feature between ego vehicle and neighbors, since their representations are then queried under different heuristics in *Level 2*) and 4). The temporal Transformer for candidate route waypoints is represented as:

$$\text{Trans}_T^P(\mathbf{X}, \mathbf{M}) = \text{MLP}(\text{concat}(\text{MHA}(\mathbf{X}, \mathbf{M}), \mathbf{Emb})). \quad (5)$$

We omitted the position embedding input, since both \mathcal{M}_t and \mathcal{K}_t carries dense positional relations themselves. The output dynamics embedding can be represented as:

$$D_{M_t}^i = \text{Trans}_T^M(M_t^i, \mathbf{M}_M^i), \quad d_{k_t}^i = \text{Trans}_T^P(k_t^{i,j}, \mathbf{M}_{k_j}^i), \quad (6)$$

where $i \in \text{ego}, 1, 2, \dots, n$ stands for all vehicles (ego and neighbors from 1 to n), and $j \in 1, 2, \dots$ is the number of candidate waypoints for each vehicle. Trans_T^M and Trans_T^L denote separated temporal Transformers, encoding historical motions and all candidate route waypoints of each vehicle $M_t^i, K_t^i = \{\mathbf{k}_t^1, \mathbf{k}_t^2, \dots\}$ with temporal masks $\mathbf{M}_M^i, \mathbf{M}_K^i = \{\mathbf{M}_{k1}^i, \mathbf{M}_{k2}^i, \dots\}$. The first stage outputs latent representations for vehicle motion dynamics $D_{M_t}^i$, and matching latent sets for candidate waypoints: $D_{K_t}^i = \{d_{k_t}^{i,1}, d_{k_t}^{i,2}, \dots\}$.

2) *Cross Modality Level*: The second stage seeks to abstract the interaction between neighboring vehicles' motion state $D_{M_t}^i$ and their local waypoint $D_{K_t}^i$. This level is modeled under the real-world heuristic that there is no cooperation among neighboring vehicles, hence the future waypoints are solely queried by their own historical motion dynamics. The cross-modality Transformer is designed along the axis of prediction numbers as follows:

$$\text{Trans}_C(\mathbf{X}, \mathbf{Y}, \mathbf{M}) = \text{MLP}(\text{MHA}(\mathbf{X}, \mathbf{Y}, \mathbf{M})), \quad (7)$$

where cross-modality inputs $\mathbf{X} = \mathbf{Q}, \mathbf{Y} = \mathbf{K}, \mathbf{V}$ and mask \mathbf{M} . The cross-modality dynamic is represented as:

$$C_t^i = \text{Trans}_C^C(D_{M_t}^i, \text{concat}(D_{K_t}^i, \mathbf{M}_k^i)) + D_{M_t}^i, \quad (8)$$

where $i = 1, 2, \dots, n$. The residual connection is added to emphasize the dynamic $D_{M_t}^i$ of neighbor vehicles, while preserving the information flow in cases unavailable for K_t^n .

3) *Aggregating Level*: The third stage focus on the high-level interactions of ego vehicle for decision-making with other neighbor vehicles. It is still assumed that in the scene, there is no interaction among neighbor vehicles. Thus in this top-level, the scene representation is encoded by aggregation with the ego dynamic itself $D_{M_t}^{\text{ego}}$ and the cross-modality output $\{C_t^1, \dots, C_t^n\}$ for neighbor vehicles, the structure also follows the cross attention scheme:

$$A_{g_t} = \text{Trans}_C^A(D_{M_t}^{\text{ego}}, \text{concat}(D_{M_t}^{\text{ego}}, C_t^1, \dots, C_t^n), \mathbf{M}_n). \quad (9)$$

4) *Output Level*: The output stage also counts the future heuristic for the ego vehicle, which should be determined through interaction awareness of neighbor vehicles. The intuition is to query the candidate route waypoints given ego dynamics and its interactions with surrounding neighbors which also have knowledge for their future intentions. Another cross-attention Transformer is designed to model this intention:

$$h_t = \text{Trans}_C^E(A_{g_t}, \text{concat}(D_{K_t}^{\text{ego}}, \mathbf{M}_k^{\text{ego}})) + A_{g_t}. \quad (10)$$

The final representation h_t is also passed through a residual connection in the output level. It is a well-structured representation given all the interactions from different levels of the input state.

C. Soft actor-critic

We implements Soft Actor-Critic (SAC) for decision-making given latent representation $h_t \leftarrow \Phi(s_t)$ through the MST structure. SAC is a model-free off-policy RL method with state-of-the-art performance in continuous decision-making tasks [30]. Its objective maximizes both cumulative

rewards and entropy with a temperature parameter α to regularize the exploration-exploitation process:

$$\mathbb{E}_{s_t, a_t \sim \pi} [\sum_t \mathcal{R}(s_t, a_t) + \alpha \mathcal{H}(\pi(\cdot|s_t))]. \quad (11)$$

SAC simultaneously learns a stochastic policy network π_ϕ (actor) and double Q-function networks $Q_{\theta_1}, Q_{\theta_2}$ for variance reduction of the Q values (critic). Given the latent representation h_t , the Q-function networks are updated according to the mean Bellman squared error (MBSE) over MDP tuples $\tau = (s_t, a_t, r_t, s_{t+1}, \gamma)$ sampled from replay buffer \mathcal{D} :

$$\mathcal{L}_c(\theta_i) = \mathbb{E}_{\tau \sim \mathcal{D}} [(Q_{\theta_i}(h_t, a_t) - (r_t + \gamma y_Q))^2], \quad (12)$$

where $i = 1, 2$, latent scene representations $h_t \leftarrow \Phi(s_t)$ is acquired through MST. The temporal difference (TD) target y_Q for soft Q-function update is given by MDP tuples τ above and actions a' sampled by current policy π :

$$y_Q = \mathbb{E}_{a' \sim \pi} \left[\min_{i=1,2} Q_{\bar{\theta}_i}(\bar{h}_{t+1}, a') - \alpha \log \pi_\phi(a'|h_{t+1}) \right], \quad (13)$$

where $h_{t+1} \leftarrow \Phi(s_{t+1}), \bar{h}_{t+1} \leftarrow \bar{\Phi}(s_{t+1})$. In the critic, target Q-values and its representations \bar{h}_{t+1} are acquired through the target network $\bar{\Phi}$ which is dynamically updated by Polyak averaging at each gradient step. The minimum Q-value from double Q networks $\bar{\theta}_{1,2}$, is taken to prevent overestimating issues for state action values.

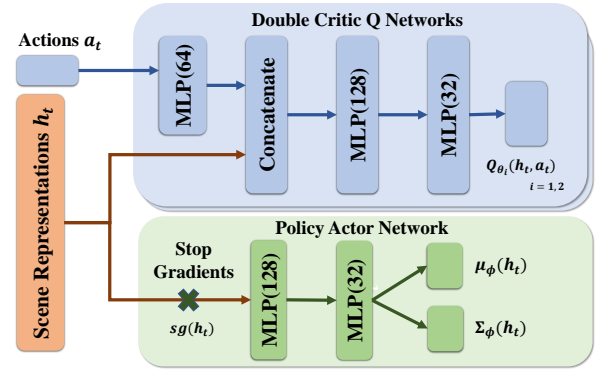


Fig. 4. The structure of Actor-Critic networks. For continuous decision-making tasks, the policy is modeled by multivariate Gaussian with mean and covariance diagonal.

The actor policy network outputs the parameters (means and covariance $\mu, \Sigma \in \mathcal{A}$) of a multivariate Gaussian distribution $\mathcal{N}(\mu, \Sigma)$, each with dimensions of action space. The actor is updated by soft-Q minimization:

$$\mathcal{L}_a(\phi) = - \mathbb{E}_{\tau \sim \mathcal{D}} \left[\min_{i=1,2} Q_{\theta_i}(h_t, a_t) - \alpha \log \pi_\phi(a_t|h_t) \right], \quad (14)$$

where the policy is taken from the state representation from the MST but stopping gradient backpropagation: $h_t \leftarrow sg(\Phi(s_t))$. The parameter α controls the trade-off of the entropy term. is automatically tuned over the course of training according to [30]. Actions are sampled from the current policy $a_t \sim \pi_\phi(\cdot|\Phi(s_t))$ during training and take the mean of policy $a_t = \mu_\phi(\cdot|\Phi(s_t))$ during testing.

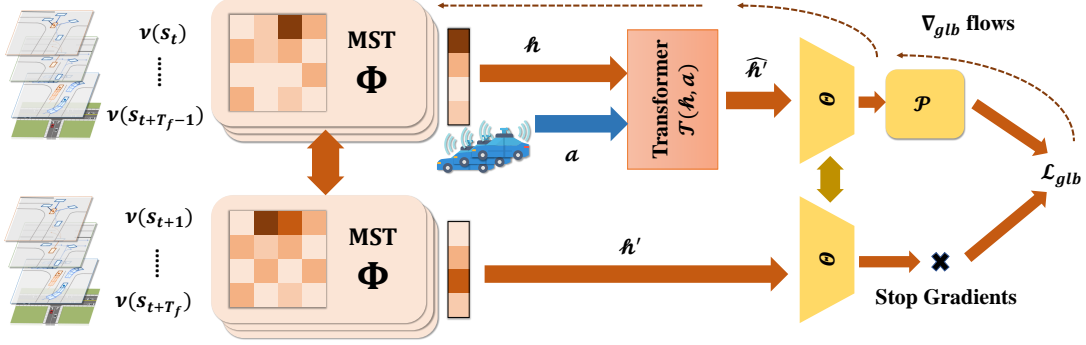


Fig. 5. The computational flow of Sequential Latent Transformer. Sequential consistent features among future horizons T_f are captured through this Siamese network structure. All augmented future states are encoded by MST Φ . It then follows a sequential representation learning with representation transition model \mathcal{T} and acquires projected similarity loss \mathcal{L}_{glb} for this auxiliary task.

D. Sequential Latent Transformer

From a global perspective, it is hypothesized that the decision-making process can be improved by having prior knowledge of the decision consequences. Intuitively, decision-making can be improved due to: 1) global prediction can bridge the state-action pairs in an episode, thus reducing the exploration space; 2) the attention weights for route waypoints \mathcal{K}_t can be implicitly guided by global predictions.

Therefore, we add an auxiliary task to better learn the latent representations h_t , which is to predict the next-step state h_{t+1} conditioned on current actions a_t during the training process. It could be modeled as a forward environment transition:

$$h'_{t+1} \leftarrow \mathcal{T}(h_{t+1}|h_t, a_t). \quad (15)$$

Nonetheless, a one-step forward model confronts three problems: 1) representations are sequentially dependent, and thus the consequence is mostly led by a series of actions rather than a single step; 2) the highly-dynamic nature of the driving scene requires distilling the sequential representations to combat the variances; 3) the current auto-encoder method causes great errors in simple state reconstruction, not to mention the sophisticated urban states. Therefore, a sequential latent transformer (SLT) is proposed as an auxiliary representation learning task during training.

To deal with the first problem, the transition model in Eq. 15 should be modified to an auto-regressive structure to model the sequential relationships among scene representations and the corresponding actions under a future horizon T_f :

$$h'_{t+k} \leftarrow \mathcal{T}_{k \leq T_f}(h_{t+k}|h_{<t+k}, a_{<t+k}). \quad (16)$$

For the second problem, a representation learning method that dominates the area of computer vision is introduced. By computing the projected latent similarity among different aspects of the same state-input through a Siamese network, the framework captures the invariant features from different aspects of inputs. For global predictions, we are able to distill the core consistent feature by inputting continuous future transition pairs. The representations then become global predictive for the transitions above. Note that the third problem is also solved since the method is reconstruction-free. To combat the variance issue, we follow the representation learning method

[31], which augments the input $v(s_t)$ to reduce the variance by averaging the same representation with different aspects of augmentations. It is also beneficial to decision-making since the Q-value over-estimation issues would be regularized with the same Q-value over different aspects of state inputs [25].

SLT Computational Framework: Fig. 5 shows the structure of SLT, which follows a SimSiam-style representation learning method [31]. Given the continuous state-action pairs over future horizon T_f :

$$(v(s_t), a_t), (v(s_{t+1}), a_{t+1}), \dots, (v(s_{t+T_f}), a_{t+T_f}),$$

then all augmented states would be encoded through MST: $h_t \leftarrow \Phi(v(s_t))$. Let \mathbf{h}, \mathbf{a} denote the representations and actions sequences $h_{<T_k}, a_{<T_k}$, the future step representations can be gathered into $\mathbf{h}' = h_{t:t+T_k}$. As shown in Fig. 6, the predicted future latent representations are acquired through an auto-regressive Transformer-based decoder: $\hat{\mathbf{h}}' = \mathcal{T}(\mathbf{h}, \mathbf{a})$. Both $\mathbf{h}', \hat{\mathbf{h}}'$ are projected with the predictor for similarity computation: $z = sg(\Theta(\mathbf{h}'))$, $\hat{z} = \mathcal{P}(\Theta(\hat{\mathbf{h}}'))$, where Θ and \mathcal{P} are MLP projector and a linear predictor, respectively. Gradient flow z is stopped for the target. The similarity loss for global predictions \mathcal{L}_{glb} is updated simultaneously with RL decision making. The implementation of SAC with the proposed Scene-Rep Transformer is given in Algorithm 1.

Similarity Loss: To prevent the representation collapse, cosine similarity is proposed as the similarity loss function [32]:

$$\mathcal{L}_{glb}(z, \hat{z}) = -\frac{z \cdot \hat{z}}{\|z\| \cdot \|\hat{z}\|}. \quad (17)$$

The loss is updated separately since all objectives do not share the same magnitude and may conflict with each other for optimization. Networks involving similarity loss computations are Φ , \mathcal{T} , Θ , and \mathcal{P} .

State Augmentation: The state augmentation v given input state s_t comprises two steps specific for driving scenarios. 1) The absolute coordinate is transformed to be Cartesian coordinate centered to ego vehicle along its longitudinal axis to focus more on the local variations. 2) All points are processed with random rotations between $[-\frac{\pi}{2}, \frac{\pi}{2}]$ by ego center to build different views for the states.

A. Urban Driving Scenarios

To validate the performance of Scene-Rep Transformer under diverse scenarios, we implement three challenging scenarios in the SMARTS, a SUMO-based simulator [33] as the experimental platform, as shown in Fig. 7. The scenarios are designed for validating the decision-making capability of the system from different aspects.

a) Unprotected left turn: The scenario is built upon the urban unsignalized T-intersection with heavy traffics. The ego autonomous driving vehicle is required to complete a left turn task without traffic signal protection, and thus the traffic flow would not stop. Starting from the 2-lanes single way minor road, the ego vehicle is required to make smart decisions across the ongoing traffic flows onto the rightmost lane on the 4-lanes two-ways major road. This scenario focuses on maneuvers for smart traffic flow crossing.

b) Double Merging: The scenario faced with is a 2-lanes merging road segment with double entrances and exits. Note that the designed traffic flow is heavier than scenario a) since for each entrance, the traffic flow is assigned for all exits. The autonomous vehicle is required to merge in from entrance A to exit B. It leaves a higher requirement for the ego vehicle to learn lane-changing focused maneuvers to finish the task.

c) Roundabout: A general city roundabout with 4 exits is designed with dense traffic flows. Entranced in crossing A, the autonomous vehicle is devised with 3 tasks with increasing difficulties to exits B, C, and D. It involves more complex decisions and longer ranges to complete the tasks.

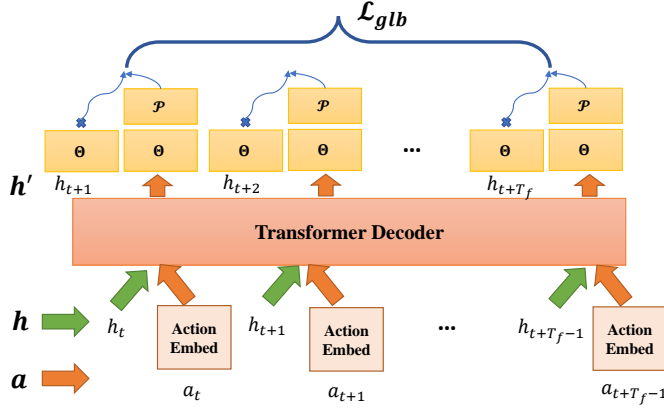


Fig. 6. The structure of the Transformer-based transition model \mathcal{T} . It is a temporal Transformer decoder given concatenated input of h_t, a_t for each timestep, and the output is representation predictions for the next step as an auto-regressive way for projections and predictions.

Data Collections: During training, we collect the transition tuples τ into replay buffer, as well as maintaining a queue \mathcal{D}^f to collect the corresponding future state-actor pairs $(s, a) = (s_{t:t+T_f}, a_{t:t+T_f})$ over the time horizon T_f .

Algorithm 1 Soft Actor-Critic with Scene-Rep Transformer

Input: Initial entropy parameter α , Polyak weight λ

- 1: Initialize MST Φ and SLT $\mathcal{T}, \Theta, \mathcal{P}$
- 2: Initialize policy network ϕ , Q value networks $\theta_{1,2}$
- 3: Initialize target networks $\bar{\Phi}, \bar{\theta}_{1,2} \leftarrow \Phi, \theta_{1,2}$
- 4: Initialize empty replay buffer \mathcal{D} , future queue \mathcal{D}^f
- 5: **repeat**
- 6: Sample ego vehicle action $a_t \sim \pi_\phi(\cdot | \Phi(s_t))$
- 7: Interact with environment $\tau = (s_t, a_t, r_t, s_{t+1})$
- 8: Store τ in deque \mathcal{D}^f
- 9: **if** $T_{epi} > T_f$ **then**
- 10: Store in buffer \mathcal{D} with $(\tau, s, a) \sim \mathcal{D}^f$
- 11: **end if**
- 12: **if** time to update **then**
- 13: Sample batch from replay buffer: $\tau, s, a \sim \mathcal{D}$
- 14: State augmentation: $s_{t:t+T_f} = v(s_{t:t+T_f})$
- 15: **RL decision making:**
- 16: Critic loss $\mathcal{L}_c = \mathcal{L}_c(\theta_1) + \mathcal{L}_c(\theta_2)$ (Eq. (12))
- 17: Polyak weight λ averaging for $\bar{\Phi}, \bar{\theta}_{1,2}$
- 18: Actor loss $\mathcal{L}_a(\phi)$ (Eq. (14))
- 19: Update entropy parameter α
- 20: **Predictive representation learning:**
- 21: Scene encoding by MST: $\mathbf{h}, \mathbf{h}' \leftarrow \Phi(s)$
- 22: Predicted transitions $\hat{\mathbf{h}}' = \mathcal{T}(\mathbf{h}, \mathbf{a})$
- 23: Projections $z = sg(\Theta(\mathbf{h}'))$, $\hat{z} = \mathcal{P}(\Theta(\hat{\mathbf{h}}'))$
- 24: Similarity loss $\mathcal{L}_{glb}(z, \hat{z})$ (Eq. (17))
- 25: Update $\mathcal{L}_c, \mathcal{L}_a(\phi), \mathcal{L}_{glb}$ with separate optimizer
- 26: **end if**
- 27: **if** s_{t+1} is terminal **then**
- 28: Reset environment, $T_{epi} = 0$
- 29: Update rest transitions in \mathcal{D}^f to \mathcal{D}
- 30: **end if**
- 31: **until** Convergence

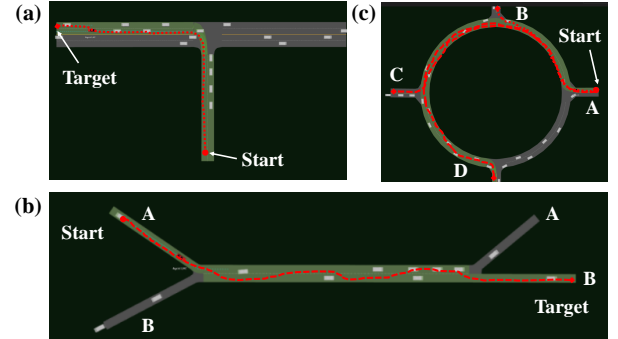


Fig. 7. The designed urban experimental scenarios in SMARTS simulator platform. a) Unprotected left turn; b) Double merging; c) Roundabout.

As shown in Fig. 7, the green color area displays the viable area for the ego vehicle to reach the target. The red dots show an example from starting route to the task target. The starting point is assigned randomly along the starting route, while the target is the endpoint for a certain route. Simulations would be reset if 1) the ego vehicle reaches the target; 2) episodic step exceeds the maximum timesteps limit; 3) the ego vehicle collides with other objects or drives off the viable routes (unable to reach the target or off the road). To construct real-world traffic flows for closer real-world simulations, multiple vehicles in traffic flows are equipped with diversified driving behaviors with randomness. In detail, for each route in the

SMARTS simulator, numerous traffic flows are assigned with a set of vehicles per flow. For each traffic flow, we randomly assign defined driving behavior models with stochasticity. Each behavior is distinctively configured by a reasonable range of randomness for parameters such as speed distribution, minimum gap, cooperation, imperfections, and impatience. The ego vehicle is also generated with randomness, and the simulation interval is set to 0.1s. More specific settings are shown in Table I.

TABLE I
SETTINGS FOR THE SIMULATED DRIVING SCENARIOS

Scenario Name	Left Turn	Double Merge	Roundabout
Max Timesteps	400	400	400/600/800
Flow rate (/h)	100	200	100
Flows (/route)	20	20	20
Vehicles (/flow)	4	4	4
Imperfection	$\mathcal{N}(U[0.3, 0.7], 0.1)$		
Impatience	$U[0, 1]$		
Cooperative	$U[0, 1]$		

B. Decision-making process

The designed state space, action space, and reward function are listed below.

1) State s : State input $s_t = [\mathcal{M}_t; \mathcal{K}_t]$ has two different modalities. For historical motion, its state space $\mathcal{S}_{\mathcal{M}} \in [n + 1, T_h, 5]$ represents the number of vehicles (ego and neighbors), historical steps, and feature dimensions. For local candidate route waypoints, its state space is $\mathcal{S}_{\mathcal{K}} = [n + 1, N_{\mathbf{k}}, T_{\mathcal{K}}, 3]$, where the second dimension indicates the maximum number of local candidate routes \mathbf{k} . It can be adjusted according to the maximum lanes for different road structures.

2) Action a : Rather than controlling the acceleration and throttle, the decision-making module outputs higher-level actions, which are executed by low-level controllers. Here, the high-level actions $a_t = [V_t, L_t]$ comprise two dimensional vectors for target speed V_t and lane changing L_t . The former is a continuous output $V_t \in [0, V_{max}]$ range from 0 to a maximum speed limit V_{max} . The latter is a discrete action $L_t \in \{-1, 0, 1\}$, where $L_t = \pm 1$ indicates a left/right lane changing, while $L_t = 0$ means to keep the lane. A low-level controller from the SMARTS simulator is employed to directly controls (both lateral and longitudinal) the ego vehicle. Note that a complete lane-changing process will take multiple steps for $L_t = \pm 1$, and otherwise will be corrected back to the current lane by the controller.

To model the hybrid actions with continuous and discrete spaces, we introduce a normalized multivariate Gaussian distribution with 2 dimensions. For $V_t \in [0, V_{max}]$, it would be normalized to $[-1, 1]$. For L_t , we discretize the second dimension of the Gaussian to 3 equal-sized bins ($[-1, -\frac{1}{3}]$ for $L_t = -1$, $[-\frac{1}{3}, \frac{1}{3}]$ for $L_t = 0$, and $[\frac{1}{3}, 1]$ for $L_t = 1$). We choose this setting because 1) the target speed should be precise as it is critical for safety; 2) speed and lane-changing decision actions are somewhat correlated.

3) Reward function $r(s, a)$: To emphasize the elevated performance for the proposed Scene-Rep Transformer frame-

work, we choose a simple and sparse goal-based reward as the reward function:

$$r_t = r_{target} + r_{penalty}, \quad (18)$$

where $r_{target} = 1$ is an indicator if the ego vehicle reaches the target, and $r_{penalty} = -1$ if the ego vehicle collides with others or drives out of the viable routes. In other cases like reaching the maximum timestep, the goal-based reward remains zero.

C. Evaluation Metrics

To make a fair evaluation of the performance of the proposed framework under different scenarios, we use the average success rate during training as the primary evaluation metric. During the test stage, we use additional metrics, i.e., the collision rate and stagnation rate.

- **Success rate (Succ.%):** It quantifies the percentage of episodes that the ego vehicle successfully reaches the target. During testing, we measure the success rate over the total testing episodes. For training cases, the success rate is measured over the last 20 episodes.
- **Collision rate (Coll.%):** It counts the percentage of episodes that the ego vehicle collides with others, which is a critical indicator for the safety performance.
- **Stagnation (Stag.%):** It counts the proportion of episodes that the ego vehicle stays still and exceeds the maximum time limit, which indicates the degree of conservativeness.

D. Comparison baselines

To make a comprehensive evaluation of the proposed approach, we compare our SAC with Scene-Rep Transformer with other existing methods for scene representations and decision-making. The baseline methods are:

1) **Data-regularized Q-learning (DrQ)** [25]: A state-of-the-art method for image-based RL (Dr-SAC for continuous action settings). Stacked rasterized images are used for representing the scene with roads and vehicles over consecutive time steps. The images would also go through random augmentations for regularization. It employs a convolutional neural network (CNN) for encoding the state and soft actor-critic (SAC) algorithm for decision-making.

2) **Soft Actor Critic (SAC)** [30]: An RL baseline method for decision-making without the proposed scene understanding framework. It takes the same representations for the state input but uses LSTM for encoding and aggregates the information from each step.

3) **Proximal Policy Optimization (PPO)** [34]: A state-of-the-art on-policy approach for decision-making. It improves the RL policy considering the constraints to stay close to the last updated policy using surrogate actor-critic objectives within an episodic horizon. We take the most common image-based scheme as input (the same as baseline 1)).

4) **Rule-based Driver Model (RDM)** [33]: Implementation with the same behavior model as neighbor vehicles, but with deterministic settings and idealized behaviors (no imperfection).

E. Implementation details

Our proposed approach and other baseline methods (except for RDM) are all trained for 100,000 steps in each urban scenario, and each experiment is conducted 5 times with different random seeds. The neural networks for all methods are trained on a single NVIDIA RTX 2080 Ti GPU using Tensorflow and Adam optimizer with a learning rate of $1e^{-4}$, and the training process for a method in a single scenario takes roughly 2 hours. The parameters related to the experiment are listed in Table II. For each method, we take the policy network with the highest success rate during training for the subsequent testing phase.

TABLE II
PARAMETERS USED IN THE EXPERIMENT

Notation	Meaning	Value
n	Max number of neighboring vehicles	5
V_{max}	Speed limit (m/s)	10
T_h	Historical horizon	10
T_K	Route waypoints horizon	10
T_G	Global predictive horizon	3
N_k	Number of candidate route waypoints	2
γ	Discount rate	0.99
λ	Polyak averaging weight	0.005
α	Initial entropy weight	1
N_{init}	Warm-up random searching step	5000
N_{buffer}	Replay buffer capacity	20000
N_B	Batch size	32
N_{train}	Training steps	100000

V. RESULTS AND DISCUSSIONS

A. Training results

We first evaluate the training performance of the Scene-Rep Transformer together with the comparison baselines. The training results are displayed by urban scenarios, where each training curve represents the mean (solid line) and standard deviation error band of certain baselines for the average training success rate. The results are recorded every 200 steps and smoothed by exponentially moving average (EMA=0.99). Fig. 8 shows the training results of different methods in all scenarios, as well as the ablated method (SAC with only MST).

The results show that SAC with the proposed Scene-Rep Transformer achieves the best training performance in all five urban scenarios with diverse tasks. The training success rate is boosted in all scenarios, especially in the more demanding urban scenes such as roundabout-C, unprotected left turn, and double merging. Sample efficiency of the proposed method is also enhanced, displaying faster convergence in fewer training steps. The results suggest that our proposed Scene-Rep Transformer can quickly adapt to different scenarios and are capable to reach the 70% – 80% of the final success rate in merely 50% of the overall training steps. Here, we give some detailed explanations about the superior performance of our proposed method compared to the baseline methods.

Compared with on-policy RL: PPO can adapt well with fast convergence in simpler tasks such as roundabout-A (Fig. 8c), resulting in 0.7 of the average success rate and convergence only in 40k training steps. But it performs worse when

the difficulty of the task increases from longer mileage to finish or more complex traffic flows. The training curve remains flat (with an average success rate of 0.2-0.4) after initial policy improvement (20k-30k) in more difficult scenarios. It is due to that PPO can be easily trapped in the local optima during training, as the PPO driving policy is updated over a predefined horizon bounded by the historical policy. It tends to overfit the temporally advantageous trajectories and make fewer improvements later on, while such policies would result in more failures when the urban traffic flow becomes more stochastic.

Compared with off-policy RL: SAC driving policy can show satisfying stochasticity in the driving scenarios. SAC with the same state inputs as our proposed method shows a significant boost for the final success rate (0.5-0.73) compared with PPO. However, SAC leaves a long time for convergence and instability, reflected in larger variance across different trials ($\sigma > 0.1$) (see Fig. 8a, b). This is mainly caused by a deficiency in state action pairs sampling for Q-value estimation or state representations encoding.

Compared with efficient RL: DrQ improves the success rate from 10.5% to 49% compared with the SAC baseline. It utilizes the data augmentation technique so that variance for Q-value estimation can be quickly converged as it provides more aspects of states for the same Q-value. It shows a faster convergence for 40k-50k training steps to reach the same performance level by SAC baseline. However, the performance is still limited by the rasterized image inputs and CNN structure, because the image cannot explicitly model the interactions among vehicles. Thus, its final performance is close to the upper error band of SAC baseline in highly interactive scenarios such as the double merging cases (see Fig. 8b).

Compared with only MST: SAC with MST improves the success rate in all scenarios on the basis of SAC baseline, as well as the efficiency of convergence to 50% – 66% of the training steps to reach the same performance of DrQ baseline. This also suggests that the SLT in the framework can keep the consistency among sequential driving scene and their decisions. Thus the proposed method results in better performance than only MST, from 84% (Fig. 8a) in left turn scenario to 23% (Fig. 8c) in the simplest roundabout-A case. A greatly improved convergence is also an advantage of the framework, taking 40% – 60% of the training steps to reach the best performance of the DrQ method.

In summary, the performance improvement of the Scene-Rep Transformer during training could originate from three aspects. First, we incorporate the multi-stage Transformer structure (MST) to represent the interactions among the ego vehicle and its neighbors, as well as the adaptive fusion of local candidate route waypoints to represent the local intentions of the ego and neighbors for decision-making. Second, the SAC algorithm is adopted for decision making which satisfies the scholastic nature of urban scenarios. Finally, the sample efficiency is further elevated through the sequential latent transformer (SLT). The state-action exploration space is reduced by the guidance of global predictive knowledge that only retains consistent information among sequential

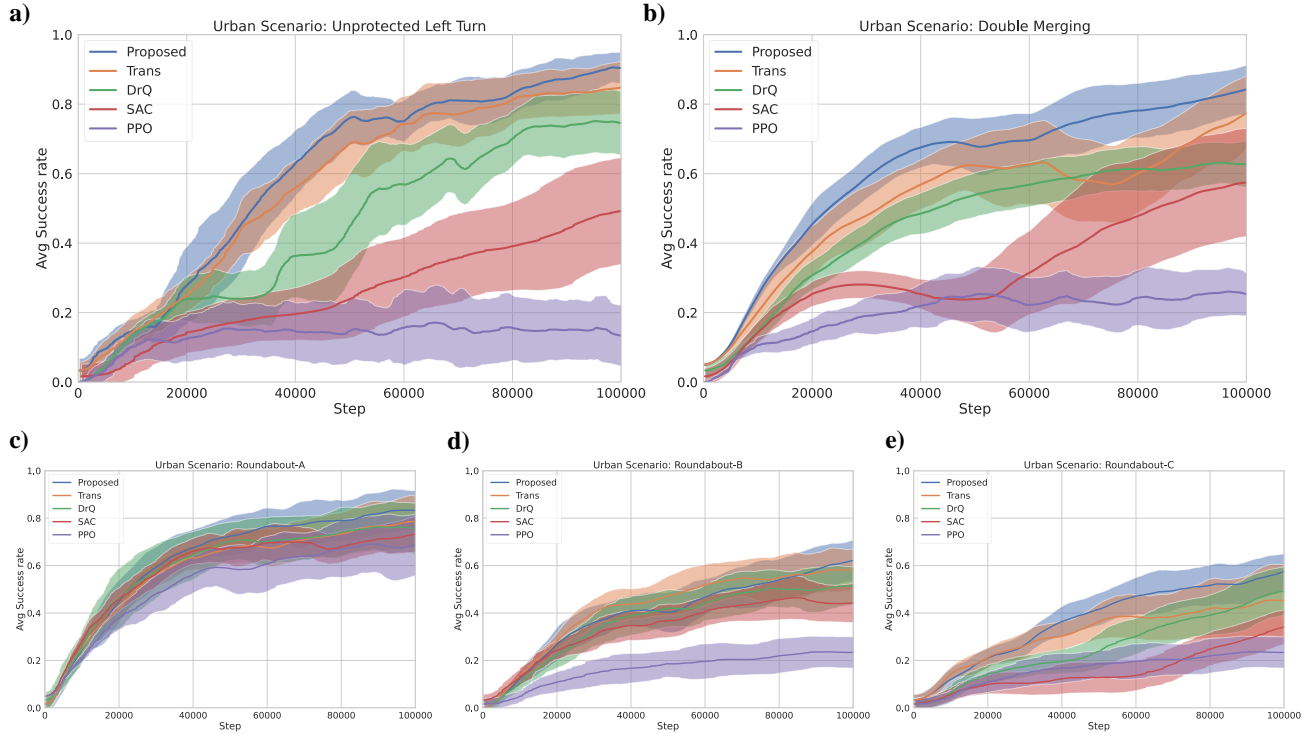


Fig. 8. The training process of our framework with baseline methods quantified by average training success rate in different urban scenarios: a) Unprotected left turn; b) Double merge; c) Roundabout-A: ego vehicle to reach Exit B; d) Roundabout-B: ego vehicle to reach Exit C; e) Roundabout-C: ego vehicle to reach Exit D. The blue curve (**Proposed**) indicates the Scene-Rep Transformer, and the orange curve (**Trans**) shows the ablative training performance with only MST. The other three training baselines are displayed in green (**DrQ**), red (**SAC**) and violet (**PPO**).

future state-action pairs in different urban scenarios, and thus convergences are boosted under limited training steps.

B. Testing results

The testing scenarios are constructed with the same road networks but different settings for parameters in Table I in terms of randomness and random seeds. The rule-based method (RDM) is also introduced during testing in comparison with other learning-based decision-making methods. Each of the following baseline and the Scene-Rep Transformer is tested for 50 episodes under each urban scenario. Statistics for three evaluation metrics (success rate, collision rate, and stagnation) during testing are presented in Table III. Note that the three metrics do not necessarily add up to 100%, as the ego vehicle agent may reach the wrong destination occasionally.

The testing results in Table III are in accordance with the training outcomes. Our proposed Scene-Rep Transformer RL framework achieves the best performance in all five urban scenarios. The proposed method brings about the highest test success rate with much fewer failure cases by collisions. Apart from the performance brought by global predictive knowledge, the capability of local predictions aided with Transformer is also verified in the MST baseline, resulting in an overall improvement compared with the DrQ baseline. However, the MST is still limited by its sole guidance for state-space compared with the guidance of both state action space sequentially through global predictions. Thus, for urban scenarios

that require long-term driving maneuvers (Roundabout-B and C in Table III) that complicate the exploration space, the performance of MST is similar to DrQ as they both merely place emphasis on the state space. The performances for SAC and PPO are alike in their training results, mainly due to their limitations illustrated in the previous section. Notably, the rule-based driver model displays terrible performance in testing, due to its inability to cope with stochastic traffic flows and collides with aggressive vehicles to cut in the ego vehicle's driving routes.

For the metric regarding driving efficiency (Stag.%), learning-based baselines show considerable performance with scarce cases of stagnation for the ego vehicle. Cases over time step limits are mainly concentrated in Roundabout-C scenarios for PPO and SAC, as it requires longer task completion time, and may stop at a traffic jam in such scenarios. The highest stagnation for inefficiency occurs from the rule-based model in the unprotected left turn. As rule-based driving agent suffers from over-conservative behaviors faced with dense traffic from the main road, the ego vehicle will remain to wait at the T-intersection until it reaches the time limit. The testing results clearly indicate that the rule-based driving model shows poor performances encountering urban scenarios with more sophisticated and stochastic settings.

To further investigate the driving efficiency of learning-based baselines with Scene-Rep Transformer, the mean and standard deviation of the completion time for successful trials

TABLE III
SUMMARY OF THE TEST RESULTS OF FIVE TESTING URBAN SCENARIOS WITH THREE EVALUATION METRICS

	Left Turn			Double Merging			Roundabout-A			Roundabout-B			Roundabout-C		
	Succ.%	Coll.%	Stag.%	Succ.%	Coll.%	Stag.%	Succ.%	Coll.%	Stag.%	Succ.%	Coll.%	Stag.%	Succ.%	Coll.%	Stag.%
RDM	2	54	44	0	100	0	6	94	0	2	98	0	0	100	0
PPO	36	50	10	36	64	0	66	34	0	42	58	0	38	50	12
SAC	68	28	0	62	22	0	76	24	0	48	52	0	46	48	6
DrQ	78	20	0	76	14	0	80	20	0	72	28	0	68	30	2
MST	88	12	0	92	4	0	84	16	0	76	24	0	66	34	0
Proposed	94	4	0	96	2	0	88	12	0	82	18	0	76	24	0

during testing episodes are computed for each urban scenario (Table IV). The results reflect the improving traveling efficiency of the proposed method under the majority of urban scenarios. It takes a longer time for PPO and SAC agents to finish the task. They both show tentative behaviors to strictly follow the routine maneuvers for PPO or act with randomness due to bias of local predictions for SAC. DrQ delivers a better traveling efficiency and lower variance owing to the data regularization mechanism during training. This is further extended by the proposed Scene-Rep Transformer through the data augmentation for multi-step future pairs, leading to similar features.

TABLE IV
TEST RESULTS OF TASK COMPLETION TIME (S)

	Left Turn	Double Merging	Roundabout		
			A	B	C
PPO	36.4±6.7	36.3±3.0	23.0±4.9	43.5±1.8	63.5±1.7
SAC	19.2±0.5	34.9±1.9	25.2±1.3	44.0±1.1	60.7±1.4
DrQ	18.2±0.4	34.9±1.7	22.4±0.3	40.3±0.5	57.4±1.8
MST	17.3±2.9	30.9±2.5	28.3±3.3	35.3±1.9	58.5±2.2
Proposed	12.5±0.4	28.6±0.6	24.5±1.2	33.7±1.2	56.6±2.2

C. Ablation study

To explore the roles of predictive representation learning and candidate route waypoints in Scene-Rep Transformer, an ablation study is conducted. Two ablative baselines are set up with partial components upon trained MST model: 1) **Ego**: MST that removes output level Transformer for the ego vehicle’s route waypoints $D_{K_t}^{ego}$; 2) **Neighbors**: MST that removes all components related to \mathcal{K}_t . All ablative baselines are tested with identical testing setups in Section V-B, and the results are displayed in Table V.

The results of the Ego baseline imply that candidate route waypoints \mathcal{K}_t^{ego} is the key for performance improvement of MST compared with efficient RL baseline such as DrQ. This is because the ego agent’s route waypoints offer a filtered area for the ego vehicle to present the driving intention given information of neighbor vehicles and their corresponding intentions (\mathcal{K}_t^n), enhancing the scene understanding ability. Therefore, there is a significant performance drop without \mathcal{K}_t^{ego} in these scenarios that have multiple potential intentions (Left Turn). Moreover, the poor results from Neighbors baseline indicate that scene understanding is more dependent on \mathcal{K}_t^n in the case of MST, as the local intentions for neighboring vehicles are more informative to the ego agent’s decision-making. The

TABLE V
ABLATIVE STUDIES FOR PROPOSED FRAMEWORK

		Proposed	MST	Ego	Neighbors	SAC
Left Turn	Succ.%	94	88	78	56	68
	Coll.%	4	12	20	36	28
Double Merging	Succ.%	96	92	90	72	62
	Coll.%	2	4	4	25	22
Roundabout-A	Succ.%	88	84	82	68	76
	Coll.%	12	16	14	32	24
Roundabout-B	Succ.%	82	76	72	44	48
	Coll.%	18	24	28	56	52
Roundabout-C	Succ.%	76	66	62	34	46
	Coll.%	24	34	38	64	48

results of attention weights in Fig. 10 indicate that multi-stage Transformer-based structure is the key to having the capability to understand intentions and interactions in urban scenes with adaptive information flow by attention.

The role of global predictive representation learning lies in its guidance for lessening the state-action exploration space $\mathcal{S} \times \mathcal{A}$. Trained by an auxiliary representation learning objective through SLT, the latent representations h_t for decision-making would share the sequential consistent features conditioned on actions. It can discover the overall picture of Q-value and lessen state-action space, lifting the sample efficiency of policy π simultaneously. Therefore, the improvement of driving policy is reflected in 1) better quantitative performance (Table IV, Table V); 2) more diversified driving maneuvers to reach the destination. The former is counted on the fact that the global prediction guides the ego vehicle’s policy to discover the advantageous regions of Q-value more efficiently. The latter is inferred by the fact that there are possibly multiple optimal trajectories for driving maneuvers to reach the destination within close time steps.

To further justify the former claim of Q-value efficiency, the Q-value after global prediction learning should be more separable with plain MST in the exploration space. Therefore, a PCA is conducted given the mean concatenate inputs for double Q-networks representing all possible explorations in $\mathcal{S} \times \mathcal{A}$ and mean of the matching Q-values. For visualization, the first two components of PCA as represented for the concatenate input by state and action. The results in Fig. 11 show a better separating capability of the proposed method with MST only, thus confirming the previous claim.

To manifest the latter claim for global predictive knowledge, trajectories of successful trials during testing are collected and shown in Fig. 9. The driving trajectories in each urban scenario

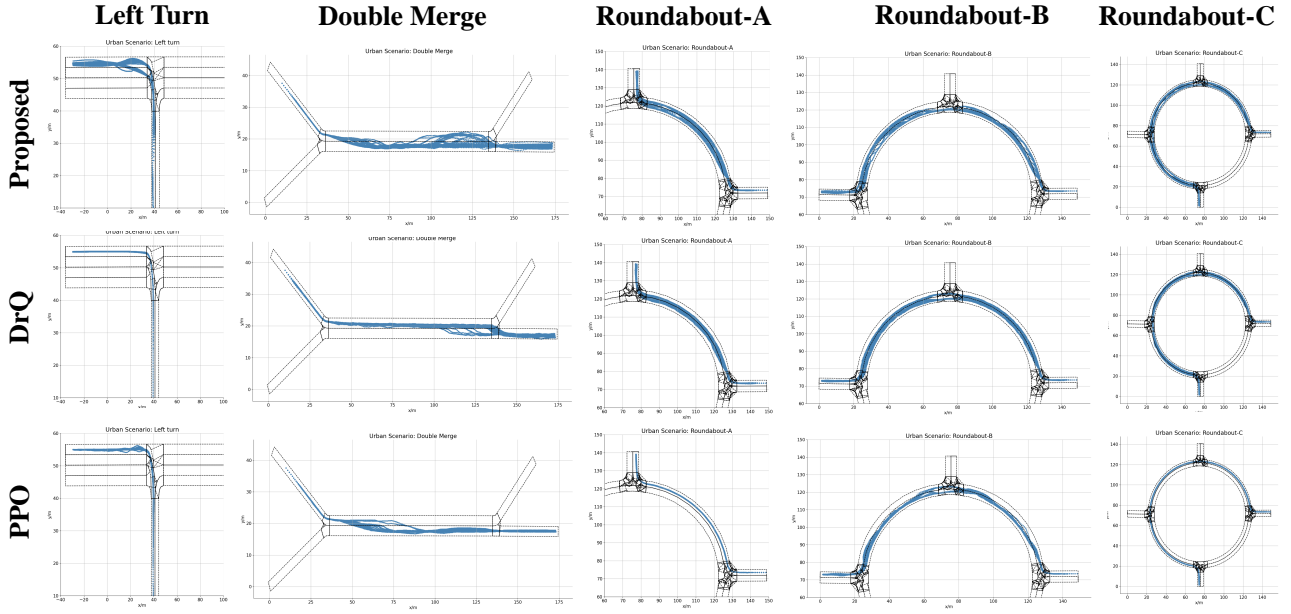


Fig. 9. The trajectories of the autonomous vehicle that successfully complete the given tasks during testing stage. The column indicates the five different urban scenarios while the row is for comparison of our method with DrQ and PPO. The trajectory distribution implies the attentioned predictive information in Scene-Rep Transformer endows more diversified long-term policies (trajectories) for task completion.

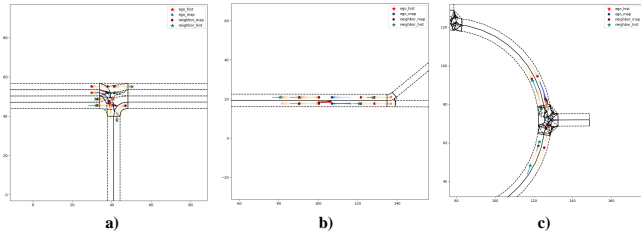


Fig. 10. Attention visualization results in a) unprotected left turn, b) double merging, c) roundabout. The information with intentions by candidate waypoints and interactions are adjusted with adaptive information flows through the multi-stage Transformer.

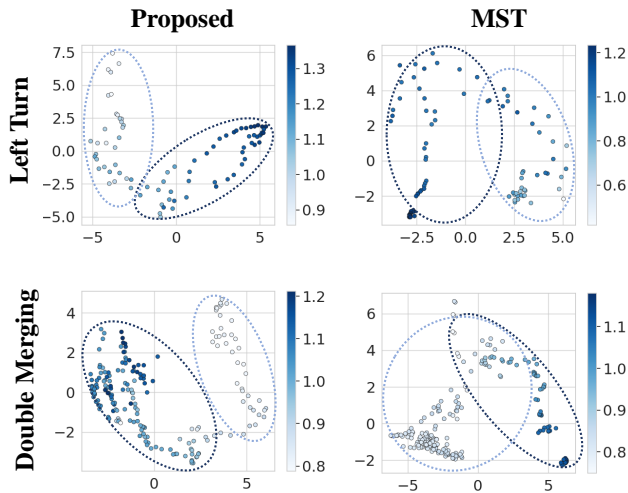


Fig. 11. Principle Component Analysis (PCA) of the first two dimensions of the learned latent representation $S \times \mathcal{A}$ by Scene-Rep Transformer and MST only. The color bar for each point is mapped with the corresponding mean Q-value by double Q-networks.

corroborate the claim of the diversity of driving maneuvers. For instance, the ego vehicle in unprotected left turn learns not only a "shortcut" to turning left to the inner lane and executes lane changing, but also a direct left turn to the second lane. More frequent lane changing occurs in different positions of the task for double merging and roundabout. Notably, the driving trajectories are more aligned with the center of each lane compared with DrQ which also displays somewhat diversity in certain urban scenarios. This characteristic might be owing to the center waypoint information by local predictions. For PPO, the previous claim for overfitted maneuvers is also verified by the monotonous trajectory distribution of PPO.

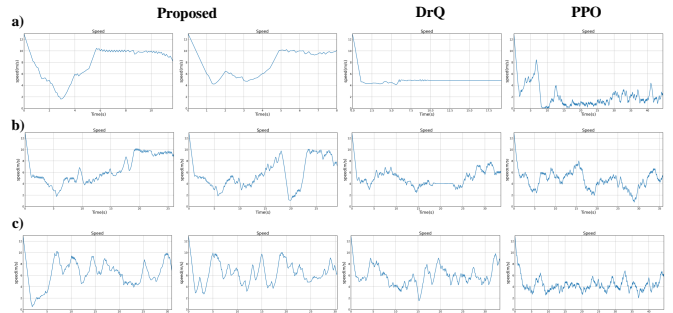


Fig. 12. Principle speed patterns of ego vehicle for successful testing trials by Scene-Rep Transformer, DrQ, and PPO baseline. Three methods are tested in a) Unprotected left turn; b) Double Merging; c) Roundabout-B.

The diversity of driving maneuvers is also reflected by the bountiful patterns of vehicle dynamic states displayed in Fig. 12. At least two significant patterns can be seen for Scene-Rep Transformer. For instance, in unprotected left turn (Fig. 12a), the ego vehicle has learned the conservative dynamic patterns to nudge with a low speed in the intersection, change the lane,

and remain a constant high speed after changing to the second lane. It has also learned an aggressive manner without lane change. For the merging cases, the ego vehicle is capable of frequent lane changing to reach the destination, or just conduct a single lane change and wait for the front vehicle but reach the destination at similar time steps. The performances of DrQ and PPO baselines are alike and incompetent, as they cannot effectively reduce the exploration space.

VI. CONCLUSIONS AND FUTURE WORK

In this paper, we propose the Scene-Rep Transformer, a novel Transformer network-based representation learning framework, to boost the sample efficiency and performance of RL decision-making. The framework consists of two main blocks: multi-stage Transformer for encoding the multi-modal scene state input and acquiring the representation understanding of the interactive driving scenes, and sequential latent Transformer for distilling the sequential predictive information into the current latent vector, to guide the decision-making process. A soft actor-critic (SAC) decision-making module takes as input the refined latent representation and outputs driving actions. All the modules are integrated and trained end-to-end with the aim to obtain a higher reward and success rate. Extensive validation is conducted with five challenging simulated urban driving scenarios. Both quantitative and qualitative results reflect the overall superior performance of the proposed method in terms of sample efficiency, testing performance, interpretability, and diversity of driving maneuvers. We also investigate the effects of different components in the framework and find that the multi-stage Transformer is adaptively aware of intentions and interactions between agents and map, and the sequential latent Transformer can effectively reduce the exploration space.

Future work will be focused on improving or dynamically adjusting the depth of global latent predictions, so as to reduce the noise induced by longer-term predictions. The prediction uncertainties should also be explicitly considered.

REFERENCES

- [1] Z. Huang, J. Wu, and C. Lv, "Driving behavior modeling using naturalistic human driving data with inverse reinforcement learning," *IEEE Transactions on Intelligent Transportation Systems*, 2021.
- [2] L. Zhu, F. R. Yu, Y. Wang, B. Ning, and T. Tang, "Big data analytics in intelligent transportation systems: A survey," *IEEE Transactions on Intelligent Transportation Systems*, vol. 20, no. 1, pp. 383–398, 2018.
- [3] E. Yurtsever, J. Lambert, A. Carballo, and K. Takeda, "A survey of autonomous driving: Common practices and emerging technologies," *IEEE access*, vol. 8, pp. 58 443–58 469, 2020.
- [4] B. R. Kiran, I. Sobh, V. Talpaert, P. Mannion, A. A. Al Sallab, S. Yogamani, and P. Pérez, "Deep reinforcement learning for autonomous driving: A survey," *IEEE Transactions on Intelligent Transportation Systems*, 2021.
- [5] Z. Huang, J. Wu, and C. Lv, "Efficient deep reinforcement learning with imitative expert priors for autonomous driving," *IEEE Transactions on Neural Networks and Learning Systems*, 2022.
- [6] J. Wu, Z. Huang, W. Huang, and C. Lv, "Prioritized experience-based reinforcement learning with human guidance: Methodology and application to autonomous driving," *arXiv preprint arXiv:2109.12516*, 2021.
- [7] S. Aradi, "Survey of deep reinforcement learning for motion planning of autonomous vehicles," *IEEE Transactions on Intelligent Transportation Systems*, 2020.
- [8] J. Chen, B. Yuan, and M. Tomizuka, "Model-free deep reinforcement learning for urban autonomous driving," in *2019 IEEE intelligent transportation systems conference (ITSC)*. IEEE, 2019, pp. 2765–2771.
- [9] Z. Huang, C. Lv, Y. Xing, and J. Wu, "Multi-modal sensor fusion-based deep neural network for end-to-end autonomous driving with scene understanding," *IEEE Sensors Journal*, vol. 21, no. 10, pp. 11 781–11 790, 2020.
- [10] J. Chen, B. Yuan, and M. Tomizuka, "Deep imitation learning for autonomous driving in generic urban scenarios with enhanced safety," in *2019 IEEE/RSJ International Conference on Intelligent Robots and Systems (IROS)*. IEEE, 2019, pp. 2884–2890.
- [11] J. Wu, Z. Huang, C. Huang, Z. Hu, P. Hang, Y. Xing, and C. Lv, "Human-in-the-loop deep reinforcement learning with application to autonomous driving," *arXiv preprint arXiv:2104.07246*, 2021.
- [12] H. Liu, Z. Huang, and C. Lv, "Improved deep reinforcement learning with expert demonstrations for urban autonomous driving," *arXiv preprint arXiv:2102.09243*, 2021.
- [13] P. Wolf, C. Hubschneider, M. Weber, A. Bauer, J. Härtl, F. Dürr, and J. M. Zöllner, "Learning how to drive in a real world simulation with deep q-networks," in *2017 IEEE Intelligent Vehicles Symposium (IV)*. IEEE, 2017, pp. 244–250.
- [14] J. Duan, S. E. Li, Y. Guan, Q. Sun, and B. Cheng, "Hierarchical reinforcement learning for self-driving decision-making without reliance on labelled driving data," *IET Intelligent Transport Systems*, vol. 14, no. 5, pp. 297–305, 2020.
- [15] Z. Huang, X. Mo, and C. Lv, "Multi-modal motion prediction with transformer-based neural network for autonomous driving," *arXiv preprint arXiv:2109.06446*, 2021.
- [16] J. Gao, C. Sun, H. Zhao, Y. Shen, D. Anguelov, C. Li, and C. Schmid, "Vectornet: Encoding hd maps and agent dynamics from vectorized representation," in *Proceedings of the IEEE/CVF Conference on Computer Vision and Pattern Recognition*, 2020, pp. 11 525–11 533.
- [17] J. Ngiam, B. Caine, V. Vasudevan, Z. Zhang, H.-T. L. Chiang, J. Ling, R. Roelofs, A. Bewley, C. Liu, A. Venugopal *et al.*, "Scene transformer: A unified multi-task model for behavior prediction and planning," *arXiv e-prints*, pp. arXiv–2106, 2021.
- [18] M. Hügler, G. Kalweit, M. Werling, and J. Boedecker, "Dynamic interaction-aware scene understanding for reinforcement learning in autonomous driving," in *2020 IEEE International Conference on Robotics and Automation (ICRA)*. IEEE, 2020, pp. 4329–4335.
- [19] P. Cai, H. Wang, Y. Sun, and M. Liu, "Dq-gat: Towards safe and efficient autonomous driving with deep q-learning and graph attention networks," *arXiv preprint arXiv:2108.05030*, 2021.
- [20] Y. Liu, J. Zhang, L. Fang, Q. Jiang, and B. Zhou, "Multimodal motion prediction with stacked transformers," in *Proceedings of the IEEE/CVF Conference on Computer Vision and Pattern Recognition*, 2021, pp. 7577–7586.
- [21] A. Prakash, K. Chitta, and A. Geiger, "Multi-modal fusion transformer for end-to-end autonomous driving," in *Proceedings of the IEEE/CVF Conference on Computer Vision and Pattern Recognition*, 2021, pp. 7077–7087.
- [22] D. Graves, N. M. Nguyen, K. Hassanzadeh, and J. Jin, "Learning predictive representations in autonomous driving to improve deep reinforcement learning," *arXiv preprint arXiv:2006.15110*, 2020.
- [23] Y. Xiao, F. Codevilla, C. Pal, and A. M. López, "Action-based representation learning for autonomous driving," *arXiv preprint arXiv:2008.09417*, 2020.
- [24] J.-B. Grill, F. Strub, F. Altché, C. Tallec, P. Richemond, E. Buchatskaya, C. Doersch, B. Avila Pires, Z. Guo, M. Gheshlaghi Azar *et al.*, "Bootstrap your own latent—a new approach to self-supervised learning," *Advances in Neural Information Processing Systems*, vol. 33, pp. 21 271–21 284, 2020.
- [25] D. Yarats, I. Kostrikov, and R. Fergus, "Image augmentation is all you need: Regularizing deep reinforcement learning from pixels," in *International Conference on Learning Representations*, 2020.
- [26] A. Srinivas, M. Laskin, and P. Abbeel, "Curl: Contrastive unsupervised representations for reinforcement learning," *arXiv preprint arXiv:2004.04136*, 2020.
- [27] T. Wang, Y. Luo, J. Liu, R. Chen, and K. Li, "End-to-end self-driving approach independent of irrelevant roadside objects with auto-encoder," *IEEE Transactions on Intelligent Transportation Systems*, vol. 23, no. 1, pp. 641–650, 2020.
- [28] K. Chen, L. Hong, H. Xu, Z. Li, and D.-Y. Yeung, "Multisiam: Self-supervised multi-instance siamese representation learning for au-

- tonomous driving,” in *Proceedings of the IEEE/CVF International Conference on Computer Vision*, 2021, pp. 7546–7554.
- [29] M. Schwarzer, A. Anand, R. Goel, R. D. Hjelm, A. Courville, and P. Bachman, “Data-efficient reinforcement learning with self-predictive representations,” *arXiv preprint arXiv:2007.05929*, 2020.
- [30] T. Haarnoja, A. Zhou, K. Hartikainen, G. Tucker, S. Ha, J. Tan, V. Kumar, H. Zhu, A. Gupta, P. Abbeel *et al.*, “Soft actor-critic algorithms and applications,” *arXiv preprint arXiv:1812.05905*, 2018.
- [31] X. Chen and K. He, “Exploring simple siamese representation learning,” in *Proceedings of the IEEE/CVF Conference on Computer Vision and Pattern Recognition*, 2021, pp. 15 750–15 758.
- [32] C. Gelada, S. Kumar, J. Buckman, O. Nachum, and M. G. Bellemare, “Deepmdp: Learning continuous latent space models for representation learning,” in *International Conference on Machine Learning*. PMLR, 2019, pp. 2170–2179.
- [33] M. Zhou, J. Luo, J. Vilella, Y. Yang, D. Rusu, J. Miao, W. Zhang, M. Alban, I. Fadakar, Z. Chen *et al.*, “Smarts: Scalable multi-agent reinforcement learning training school for autonomous driving,” *arXiv preprint arXiv:2010.09776*, 2020.
- [34] J. Schulman, F. Wolski, P. Dhariwal, A. Radford, and O. Klimov, “Proximal policy optimization algorithms,” *arXiv preprint arXiv:1707.06347*, 2017.